AIAA JOURNAL
Vol. 46, No. 6, June 2008

Harmonic Solution of Unsteady Flow Around Blades with Separation

L. He*
University of Durham, Durham, England DH1 3HP, United Kingdom

DOI: 10.2514/1.28656

Conventional time-linearized harmonic methods using a pseudo-time-marching technique often exhibit solution divergence behavior for highly loaded conditions with flow separation. This is attributed to the growth of linear instabilities associated with small-scale limit-cycle oscillations of the base-flow state. In the present work, an alternative harmonic formulation is adopted for modeling harmonic disturbances with an intention to harness nonlinearity as a means of stabilization while achieving the same computational efficiency as a conventional time-linearized model. One unsteady complex-number harmonic solution is made equivalent to two real-number steady-flow solutions with simple source terms, whereas nonlinearity is retained in the convective fluxes of discretized flow equations. The validity and effectiveness of the method has been demonstrated in comparisons with semi-analytical results for a flat plate cascade and experimental data for low- and high-speed turbine cascades. The computational results show that the present harmonic solver is robust with much improved convergence over the conventional time-linearized model. It is shown that converged solutions can be effectively obtained using the present method for unsteady flows with large-scale separation.

Nomenclature

A_U, B_U	=	Fourier harmonic coefficients of flow variable
a_v, b_v	=	Fourier harmonic coefficients of mesh volume variation in time
U	=	conservative flow variables
U_0	=	steady-flow variables
$\bar{U}$	=	time-averaged flow variables
u_g	=	moving grid velocities in the axial direction
Δv	=	mesh cell volume
x	=	axial coordinate
θ	=	circumferential angle
σ	=	interblade phase angle
τ	=	pseudotime

I. Introduction

MODERN turbomachinery components are typically designed with high loading and compact configurations, leading to an increased importance of unsteady effects. Blade mechanical integrity, aerodynamic noise, and vibration stress levels need to be carefully examined when aeroloading is to be increased, and those widely used empirical design rules have been increasingly challenged. The development of efficient unsteady aerodynamic modeling methodologies has been an active research area. The main impetus to devise and develop fast and accurate modeling methods is for engineers to be able to adopt aeromechanical analysis as part of a blading design optimization process. The direct time-domain methods to solve nonlinear unsteady flowfields in multipassage and multirow domains can provide useful information and insights to help our understanding of complex unsteady-flow phenomena and mechanisms. However, it is recognized that the direct time-domain calculations for unsteady turbomachinery flows are very expensive and not suitable for applications in a design environment.

Received 1 November 2006; revision received 19 October 2007; accepted for publication 4 December 2007.

*Currently Rolls-Royce/Royal Academy of Engineering Professor of Computational Aerothermal Engineering, Department of Engineering Science, University of Oxford, Oxford, England OX1 3PJ, United Kingdom.

In a blading design optimization process, a change in aerothermal performance can be routinely evaluated by three-dimensional steady-flow solvers as found in most of advanced blading design systems. The extent to which an aeromechanical solver can be used concurrently in such a process will thus be strongly influenced by its running time in comparison to that of a steady-flow solver. There are two main elements affecting the computational efficiency of an unsteady-flow solver. Firstly, for the same number of mesh points, a time-accurate solution for blade row interaction problems would typically consume about 15–20 times more CPU than a steady solution [1]. The difference can be much more for low-frequency long wavelength (e.g., inlet distortion driven forced responses at low engine orders or blade flutter in low structural modes) problems, which require more iterations during time-marching integrations. Secondly, to model proper circumferential length scales would normally lead to use of a whole-annulus computational domain, resulting in another factor between 20 and 100. Hence, a direct time-domain nonlinear unsteady solution would typically be 2–3 orders of magnitude more time consuming than a steady-flow solution. There certainly is a need for developing efficient numerical modeling techniques.

For turbomachinery aeromechanical and aeroacoustic applications, one often needs to consider a harmonic disturbance at a given frequency. For example, for blade flutter and forced response problems, unsteady-flow disturbances are required to be predicted for a given mode shape and frequency of a particular structural mode. Similarly a harmonic solution at a given frequency is required for a tonal noise propagation of a particular acoustic mode. This requirement for a single harmonic solution, coupled with the well-established "tuned cascade" model (Lane [2]), enables extremely useful truncations to be carried out in both temporal and circumferentially spatial directions. The frequency-domain harmonic aerodynamic models for a single blade-passage domain have been extensively developed and applied. Early unsteady aerodynamics analyses adopt time-linear methods (e.g., those by Whitehead [3], Atassi and Akai [4], Adamczyk and Goldstein [5], Ni and Sisto [6], Verdon [7], and Namba [8]). The time-linearized methods in which the linear unsteady perturbations are based on nonlinear steady-flow solutions have been developed in 1980s and 1990s. Early time-linearized methods are based on a potential flow model with notable examples of Whitehead [9] and Verdon and Caspar [10]. The time-linearized Euler methods (e.g., Hall and Crawley [11] and Hall and Lorence [12]) and the Navier–Stokes methods (e.g., Clark and Hall [13] and Sbardella and Imregun [14]) have also been developed. The

computing time required for a conventional time-linearized solution for one complex-number harmonic is equivalent to that for two steady-flow solutions.

In general, the temporal Fourier series can be used to represent nonlinear periodic flows in time and in space. The Fourier modeling was initially adopted in fully nonlinear time-domain calculations in a single blade-passage domain by He [15] and others [16,17]. More recently, efforts have also been made in using the Fourier modeling for nonlinear unsteady flows in a frequency domain. The nonlinear coupling between harmonics and time-averaged flow is included in the nonlinear harmonic model by Ning and He [18]. The cross coupling among harmonics is included in a more complete harmonic balance formulation by Hall et al. [19], and a nonlinear frequency-domain harmonic method is also developed by McMullen et al. [20]. All of these nonlinear harmonic frequency-domain methods solve equivalently $2N + 1$ steady flowfields for an unsteady flowfield solution retaining N harmonics.

For highly loaded flows in blade rows at off-design (or even design) conditions, local flow separation is often unavoidable. The conditions with flow separation present a challenge to the conventional time-linearized model. The steady-flow solutions tend to exhibit an oscillatory convergence behavior. Although the convergence oscillations are typically very local and in very small scales with negligible effects on the solution accuracy of the base flow, a time-linearized solution may diverge with unbounded error growth. The behavior is caused by instabilities typically associated with flow separation in a base-flow solution, as analyzed by Campobasso and Giles [21]. A linear stability analysis will lead to an exponential growth of disturbances of the corresponding eigenmodes. Hence, a linearized solution about the base flow would diverge. The convergence difficulty can be overcome by certain numerical techniques, such as the generalized minimal residual (GMRES) method [21], but these are associated with extra complexity and memory penalties.

It is worthwhile to note that, at those separated flow conditions, the base-flow solutions would not diverge. This is because the base flow is solved using the nonlinear flow equations and, as such, the nonlinearity would limit the growth of the instability, resulting in local small-scale limit-cycle oscillations as observed. This observation points to a possibility of harnessing the nonlinearity to overcome the convergence difficulty in conventional time-linearized solutions. In the following, it will be shown that a much-improved convergence performance for unsteady harmonic solutions for flow with separation can be achieved by a relatively simple alternative harmonic formulation. Its computational efficiency is higher than nonlinear solutions and is equivalent to only two steady-flow solutions as in the conventional time-linearized approach.

II. Modeling Formulations and Solution Methods

A. Harmonic Formulation

Take a computational mesh cell (with a volume δV and bound surface δA) as a control volume. For the convenience of simulating flows in multiple rotor and stator blade rows, a cylindrical coordinate system (x, θ, r for axial, circumferential, and radial directions) is adopted. An integral form of the 3-D unsteady Navier–Stokes equations over a moving control volume (mesh cell) is

$$\frac{\partial}{\partial t}\iiint_{\delta V} U\,\mathrm{d}V + \oiint_{\delta A}[(F - V_x - Uu_g)\mathbf{n}_x + (G - V_\theta - Uv_g)\mathbf{n}_\theta + (H - V_r - Uw_g)\mathbf{n}_r]\cdot\mathbf{d}A = \iiint_{\delta V} S_i\,\mathrm{d}V \tag{1}$$

The one-equation turbulence transport model by Spalart and Allmaras [22] is adopted. Hence, the conservative flow variable U is a six-element vector for a three-dimensional unsteady flow. F, G, and H are the convective flux vectors. V_x, V_θ, and V_r are diffusive/viscous flux vectors and S_i is the source term to account for rotating effects. The details of these standard terms can be found elsewhere [23] and will not be repeated here.

The semidiscrete integral form of the equations for a 3-D mesh cell is

$$\frac{\partial}{\partial t}(U\Delta v) = -\Sigma(F_x\Delta A_x + F_\theta\Delta A_\theta + F_r\Delta A_r) + S\Delta v \tag{2}$$

where the summation is over the boundary faces of a mesh cell, with the normal projected areas in the three directions being ΔA_x, ΔA_θ, and ΔA_r, respectively. F_x, F_θ, F_r are the flux terms, including the moving grid terms, the nonlinear convective fluxes and viscous terms in the moment and energy equations. The right-hand side of Eq. (2) can be lumped together as a residual term, and the equation can be simply expressed as

$$\frac{\partial}{\partial t}(U\Delta \mathrm{v}) = R(U) \tag{3}$$

An unsteady-flow variable can be decomposed into a mean-flow part and an unsteady harmonic disturbance at a given frequency ω.

$$U = \bar{U} + A_U\cos\omega t + B_U\sin\omega t \tag{4}$$

where A_U and B_U are real-number vectors of the same dimensions as U (i.e., six for the three-dimensional flow equations with the one-equation turbulence model). For a harmonically moving grid to accommodate a blade vibration, the mesh cell volume can also be similarly expressed as

$$\Delta v = \Delta\bar{v} + a_v\cos\omega t + b_v\sin\omega t \tag{5}$$

Substitute the expressions [Eqs. (4) and (5)] for the conservative variables and cell volume into the semidiscrete form of the unsteady Navier–Stokes equations. Then we have

$$\omega[(B_U\cos\omega t - \mathrm{A}_U\sin\omega t)\Delta v + (b_v\cos\omega t - a_v\sin\omega t)U] = R(U) \tag{6}$$

Note that Eq. (6) is in the time domain and, hence, valid for any time instant (temporal phase angle). Thus, an iterative solution can be pursued at any chosen time instant, similar to the dual timing technique [24] and more closely the time-domain harmonic balance [19]. Taking advantage of this, we can take Eq. (6) at two specific phase angles, leading to two sets of equations sufficient for the solutions of two sets of harmonic coefficients, A_U and B_U.

At $\omega t = 0$ deg, denoting $U_A = \bar{U} + A_U$ and $\Delta v_A = \Delta\bar{\mathrm{v}} + a_v$, then

$$\omega(B_U\Delta v_A + U_A b_v) = R(U_A) \tag{7a}$$

At $\omega t = 90$ deg, denoting $U_B = \bar{U} + B_U$ and $\Delta v_B = \Delta\bar{v} + b_v$, then:

$$-\omega(A_U\Delta v_B + U_B a_v) = R(U_B) \tag{7b}$$

These equations at the two given temporal phase angles are no longer explicitly dependent on the physical time t. Now we introduce a pseudotime τ to enable a time-marching solution at each phase angle:

$$\frac{\partial U_A}{\partial\tau} = \frac{1}{\Delta v_0}[R(U_A) - \omega(B_U\Delta v_A + U_A b_v)] \tag{8a}$$

$$\frac{\partial U_B}{\partial\tau} = \frac{1}{\Delta v_0}[R(U_B) + \omega(A_U\Delta \mathrm{v}_v + U_B a_v)] \tag{8b}$$

It is emphasized that the residual terms $R(U)$ contain the nonlinear convective fluxes for which no truncations are made. Hence, the discretized formulations [Eq. (8)] for the harmonic unsteady-flow disturbances at the two time instants are nonlinear. (In the Appendix, the formulations of the conventional time-linearized model and the present one are given for a simple model equation for a more direct comparison.)

In general, the mean-flow state $\bar{U}$ can be different from the steady flow U_0 due to the nonlinear interaction between the mean flow and

the unsteadiness. In that case, $\bar{U}$ needs be part of the solution, and this can be achieved if we use the aforementioned procedure for another distinctive phase angle:

At $\omega t = -90$ deg, denoting $U_{-B} = \bar{U} - B_U$, then

$$\frac{\partial U_{-B}}{\partial \tau} = \frac{1}{\Delta v_0}[R(U_{-B}) - \omega(A_U \Delta v_v + U_B a_v)] \tag{9}$$

In this way, we have three equations for three unknowns $\bar{U}$, A_U, and B_U, and

$$\bar{U} = (U_B + U_{-B})/2 \tag{10}$$

The solution of a nonlinear unsteady-flow problem with one harmonic is similar to solving three sets of steady-flow equivalent equations, that is, $2N + 1$ solutions for N harmonics [19] when only one harmonic is retained.

A further simplification can be made. The formulations as given by Eq. (8) provide a convenient way for a speed up of solution. If a steady flow U_0 is given as the base flow and the nonlinear coupling between the base flow and the harmonic disturbance can be neglected, we will only need to solve two sets of equations [Eq. (8)] for the two harmonic coefficients (A_U, B_U). In doing so, it should be noted that the nonlinearity in the convective flux terms are still retained. Therefore, we can include the nonlinearity in the discretized equations for stabilizing the harmonic solutions for separated flows while maintaining the same high computational efficiency as the conventional time-linearized methods.

For situations in which a steady-flow solution convergence exhibits limit-cycle oscillations of measurable magnitudes, we should first time average the flowfield over the limit-cycle oscillations to uniquely define the base-flow state ($\bar{U}$). There is another related issue regarding the base-flow state. For a limit-cycle oscillatory flow of a measurable magnitude, the time-averaged residuals (net fluxes) will be zero, but the residuals calculated using the time-averaged flow variables are not guaranteed to be zero, due to nonlinearity [i.e., the influence of the deterministic stresses (see Adamczyk [25])], this is,

$$\overline{R(U)} = 0 \tag{11a}$$

but

$$R(\bar{U}) \neq 0 \tag{11b}$$

Equation (11a) can also be expressed in terms of the deterministic stresses term (DST):

$$R(\bar{U}) + \mathrm{DST} = 0 \tag{11c}$$

It was previously shown that the inclusion of these extra DSTs in the Navier–Stokes equations can lead to a convergence of a time-independent solution for large-scale limit-cycle type of flow instabilities, for example, trailing-edge periodic vortex shedding (Ning and He [26]). Based on these considerations, the residual imbalance in the base-flow equations can thus be accounted for by using the following formulations for the two phase angles:

$$\frac{\partial U_A}{\partial \tau} = \frac{1}{\Delta v_0}[R(U_A) - \omega(B_U \Delta v_A + U_A b_v) - R(\bar{U})] \tag{12a}$$

$$\frac{\partial U_B}{\partial \tau} = \frac{1}{\Delta v_0}[R(U_B) - \omega(A_U \Delta v_B + U_B a_v) - R(\bar{U})] \tag{12b}$$

Hence, if a "steady-state" solution exhibits a limit-cycle oscillation, we can first time average it to get the time-averaged flow variables $\bar{U}$. Then the extra residual terms $R(\bar{U})$ can be evaluated once before the time-marching solutions for (A_U, B_U). It should be pointed that the deterministic stress terms $R(\bar{U})$ are only significant when the limit-cycle oscillations are of a measurable magnitude. For the cases to be presented later, no limit-cycle oscillations of significant amplitudes are observed. Nevertheless, this extra treatment of the deterministic stresses corresponding to the limit-cycle oscillations is introduced for a completeness of the modeling in dealing with this type of problem.

B. Solution Method and Boundary Conditions

The harmonic equations at the two temporal phase angles [Eq. (12)] are solved using a time-marching flow solver. The spatial discretization is in a second-order cell-center-based finite volume scheme with a blended second- and fourth-order numerical dissipation (Jameson et al. [27]). The time-marching solution is performed by a four-stage Runge–Kutta integration in the pseudotime. The time-marching solutions are accelerated by the multigrid and local time-stepping techniques.

For a solid wall surface, as the two-phase solutions are directly carried out in the time domain, the wall conditions are the same as those for steady flows. For a Navier–Stokes solution, the nonslip wall is applied if a fine mesh is used. For coarser meshes, the slip wall condition is applied with the shear stresses being evaluated from the log law. For separated flows, the shear stresses are directly calculated from the wall velocity gradient equivalent to the nonslip wall condition. For an inviscid Euler solution, the slip-wall condition with zero normal convective fluxes is applied.

For a blade row, a single blade-passage domain is adopted. At the "periodic" boundaries, a phase-shift boundary condition is implemented, similar to that for a conventional time-linearized complex-number harmonic method. For a typical circumferential traveling wave disturbance, the flow variables at a periodic boundary point (x, θ, r) have a constant phase angle lead σ (interblade phase angle or IBPA) to those at the corresponding point (x, θ', r), which is one blade pitch apart. Then the phase-shift periodic condition can be easily implemented for the two real-number harmonic components by

$$A_\theta = A_{\theta'} \cos\sigma + B_{\theta'} \sin\sigma \tag{13a}$$

$$B_\theta = B_{\theta'} \cos\sigma - A_{\theta'} \sin\sigma \tag{13b}$$

For inlet and exit boundaries, the boundary condition treatments can use either the same reflective treatment as those for the steady-flow solutions (specifying inlet stagnation pressure, stagnation temperature, inlet flow angle, and exit static pressure) or a local characteristic disturbance-based nonreflective treatment by Giles [28].

As mentioned, time-averaged flow variables will be required to define the base-flow state if the steady-flow solution experiences a limit-cycle oscillatory pattern. A simple updating of the time-averaged flow variables at step n is used:

$$\bar{U}n = \frac{n-1}{n}\bar{U}_{n-1} + \frac{1}{n}U_n \tag{14}$$

If the number of steps for each cycle is known by inspecting an established limit-cycle pattern, then the solution can be restarted for one further period for the time averaging. Otherwise, the summation needs to be carried out for a sufficient number of steps to cover a few cycle periods.

For blade aeromechanical vibration related applications with dynamically deforming grids due to a prescribed blade motion, the mesh volumes are first worked out at the two temporal phases, $\Delta v = \Delta v_A$ at $\omega t = 0$ deg and $\Delta v = \Delta v_B$ at $\omega t = 90$ deg. Then we can obtain the harmonics of the mesh volumes (a_v and b_v) for a given mean (fixed) volume, $\Delta \bar{v} = \Delta v_0$. The assumption is that the volume variation is of a linear manner so that the mean volumes remain the same as those fixed ones in steady-flow calculations. These volume harmonics are easily calculated before the main time-marching iterations for the flow harmonics.

III. Computational Examples

A. Flat Plate Cascade Subject to Incoming Wake

For validating the basic harmonic formulations and implementation, the unsteady flow around a flat plate cascade subject to incoming unsteady wakes is computed, and the results are compared with a well-established semi-analytical linear method, LINSUB [29].

The cascade of a pitch/chord ratio of 0.5 has a 30 deg stagger angle (Fig. 1). At a zero incidence, the steady flowfield is uniform with a Mach number of 0.7. The incoming wakes in terms of the specified entropy and vorticity waves are travelling circumferentially at the same speed as the absolute flow velocity. Hence, the wakes are in an angle of −30 deg with the axial direction.

The computational domain covers a single blade passage with the upstream and downstream boundaries at one chord from the leading edge and the trailing edge, respectively. As this is an inviscid Euler solution, the mesh points are uniformly distributed throughout, with 480 mesh cells in the streamwise direction and 80 mesh cells in the tangential direction.

Assume a constant static pressure and a constant stagnation temperature relative to the wake. The inlet pitchwise distributions of a harmonic wake disturbance in terms of primitive variables are given by

$$\Delta P = P - P_0 = 0 \tag{15a}$$

$$\Delta u = u - u_0 = u_0 \delta \cos(\omega t + \sigma y) \tag{15b}$$

$$\Delta v = v - v_0 = v_0 \delta \cos(\omega t + \sigma y + \pi)] \tag{15c}$$

$$\Delta \rho = \rho - \rho_0 = \frac{(\gamma - 1)}{\gamma} \frac{\rho_0}{P_0} \left(u_0^2 + v_0^2\right) \delta \cos(\omega t + \sigma y) \tag{15d}$$

where y is the circumferential distance normalized by blade pitch spacing and σ is the interblade phase angle. δ is the nondimensional wake perturbation and is taken to be 0.01 in this case. The disturbance should be small enough so that the case is within a linear response range, whereas the unsteadiness should not be too small, to avoid rounding errors. The tangential velocity disturbance is in antiphase with the axial one due to the wake orientation. These distributions are used to specify the instantaneous incoming characteristic disturbances at the inlet for the two phase solutions at $\omega t = 0$ and 90 deg.

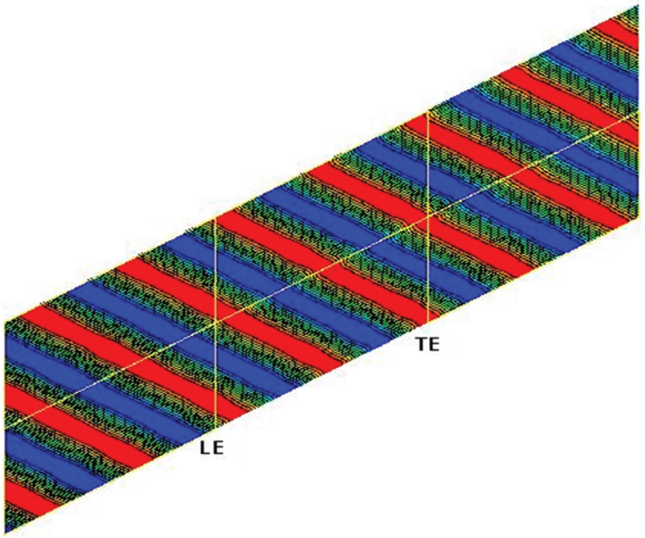

Fig. 1 Entropy contours of a flat plate cascade subject to incoming unsteady wake disturbances (two-passage domain reconstructed from a single-passage solution, IBPA $\sigma = -400$ deg).

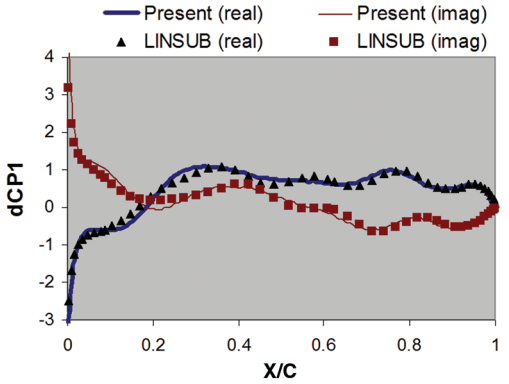

Fig. 2 Real and imaginary parts of the complex pressure jump coefficient (flat plate cascade subject to incoming unsteady wake disturbances).

As in most conventional time-linearized solutions, the results of LINSUB are in the form of complex pressure harmonics, for which a real part corresponds to A and an imaginary part corresponds to $-B$ in the present notation. The chordwise distributions of the real and imaginary parts of the complex pressure jump coefficients are shown in Fig. 2. The calculated results are in very good agreement with LINSUB.

For this case, the flow should behave completely linearly as there is no source of nonlinearity. The present modeling formulation includes certain nonlinearity, as described in Sec. II. A further calculation is made using a 3% wake velocity disturbance and the result is compared with that of a 1% wake disturbance, as shown in Fig. 3. The excellent agreement demonstrates that the present method predicts accurately a linear response of the flow to the wake disturbances as expected.

This case has also been calculated by using the conventional complex harmonic formulation as used by Chen et al. [30], giving the same results as the present harmonic solver. The convergence histories of the two methods are shown in Fig. 4. It is clear that, for this case, both the present harmonic model and the conventional linearized complex harmonic model converge well and have very similar convergence rates.

B. Low-Speed Turbine Cascade with Flow Separation

Here we consider an oscillating cascade of a realistic low-pressure turbine blading. The blading has been used in investigations of unsteady wake effects on time-averaged flow losses (Hodson and Dawes [31]) and turbine blade aeroelasticity (He [32]). The cascade flow is of particular relevance as for all of the cases tested and computed there are flow separation regions on both the pressure and the suction surfaces. A small laminar separation bubble at around 70% chord on the suction surface has only very localized effects. The

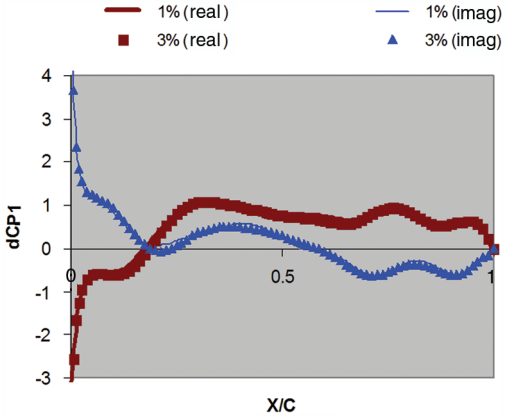

Fig. 3 Real and imaginary parts of the complex pressure jump coefficient (flat plate cascade subject to incoming unsteady wake disturbances).

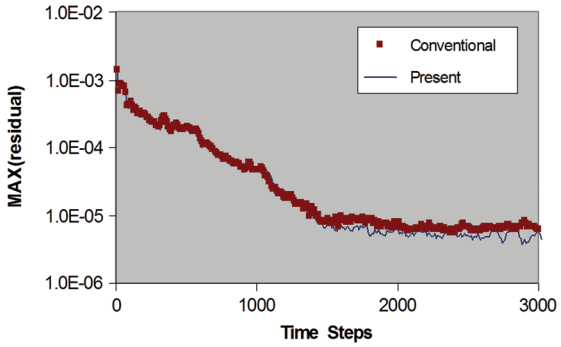

Fig. 4 Convergence histories of the present harmonic solver and a conventional time-linearized solver (flat plate cascade subject to incoming unsteady wake disturbances).

pressure surface separated region, on the other hand, can cover a large region from the leading edge to 60% chord and is shown to have a significant impact on the both steady and unsteady pressures. It is worthwhile noting, however, that even for the conditions with the largest pressure surface flow separation the computational study using a nonlinear time-domain flow solver suggests the unsteady-flow response is largely linear [32]. This case presents a challenge to the conventional time-linearized frequency-domain modeling approaches, chiefly due to the convergence difficulty associated with flow separations, rather than the modeling inaccuracy associated with the basic time-linear assumption.

The multiblock computational mesh for this 2-D turbine cascade is shown in Fig. 5, with total mesh points of 63,581 for 5 blocks in a single-passage domain. The calculated steady surface pressures for the nominal conditions (inlet flow angle of 30 deg and Reynolds number of 220,000) is shown in Fig. 6, in good agreement with the experimental data. The pressure surface large-scale separation is observed in the experiment [32] and is evident from the computation results in terms of the stagnation pressure/entropy loss (Fig. 7a) and the eddy viscosity (Fig. 7b).

The first unsteady calculation is conducted with the cascade subject to incoming wakes. The circumferential travelling harmonic disturbances are specified similarly to the case for the flat plate cascade. The incoming wakes are angled with the axial direction by 60 deg, similar to that in the study by Hodson and Dawes [31]. Contours of unsteady entropy harmonic disturbances computed by the present harmonic method are given in Fig. 8. As a wake is convected through a blade passage, it is indicated to be compressed initially due to the convection velocity difference between the suction and pressure surfaces. The "negative jet" behavior transporting the high entropy loss fluid within a wake from the pressure surface to the suction surface is visible. It is also noticeable that the wake convection is blocked by the large separation bubble.

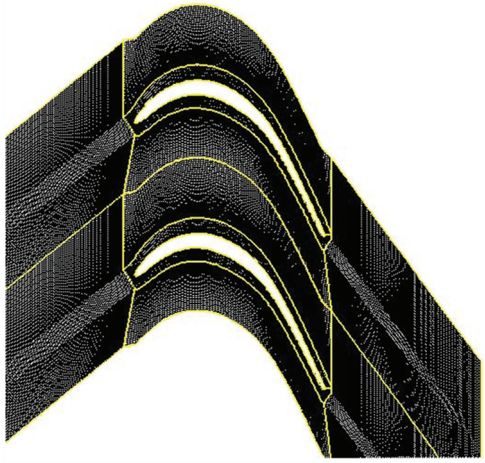

Fig. 5 Computational mesh for a low-pressure turbine cascade.

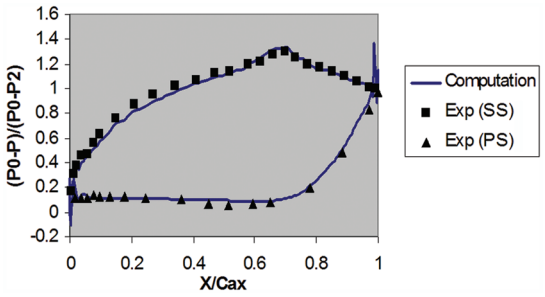

Fig. 6 Steady surface pressure distributions for a low-pressure turbine cascade (inflow angle = 30 deg).

Overall, the harmonic solution captures well the major features for such unsteady situations.

The harmonic solution is carried out based on a fixed steady base flow and, hence, requires the CPU time equivalent to two steady-flow solutions, which is comparable to a conventional time-linearized complex harmonic solution. The key difference is in the convergence. The convergence behavior is revealed in Fig. 9, which shows a converged solution can only be achieved by the present harmonic solution, whereas the conventional time-linearized model diverges very quickly.

A further examination of the present modeling and implementation is made for the oscillating cascade for blade flutter applications. Unsteady harmonic calculations for the oscillating cascade are made at inlet flow angles of 20 and 40 deg. For both inflow angles, the leading-edge separation bubble on the pressure surface is indicated

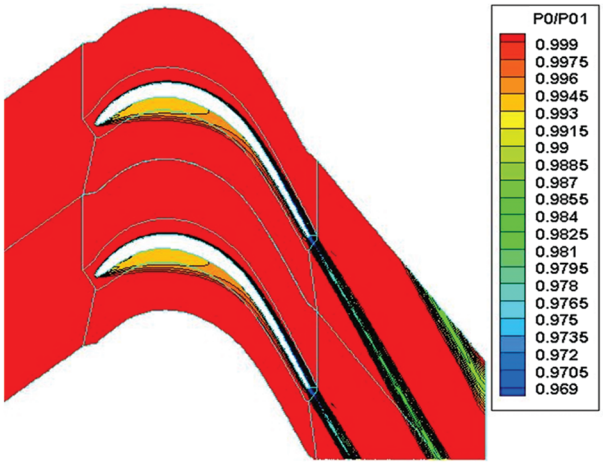

a) Total pressure loss

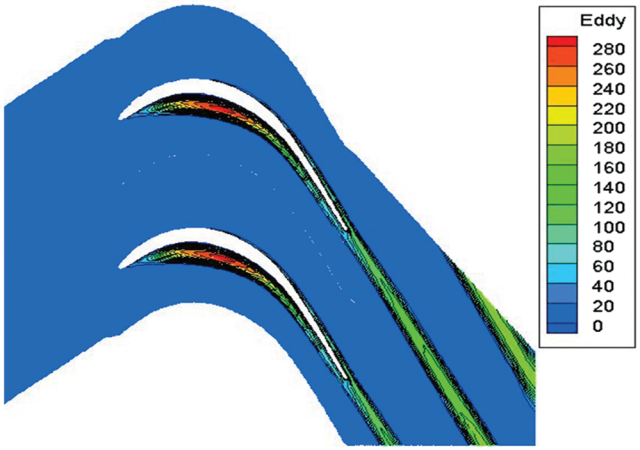

b) Turbulence eddy viscosity (normalized by laminar viscosity)

Fig. 7 Steady-flow results for a low-pressure turbine cascade (inflow angle = 30 deg).

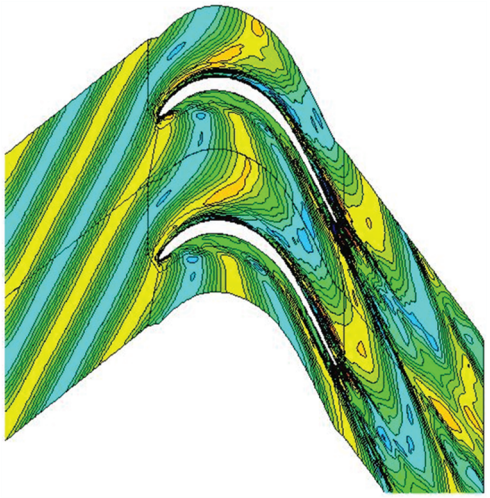

Fig. 8 Calculated harmonic entropy disturbances due to incoming wakes (low-pressure turbine cascade at a mean-flow angle of 30 deg and incoming wake angle of 60 deg).

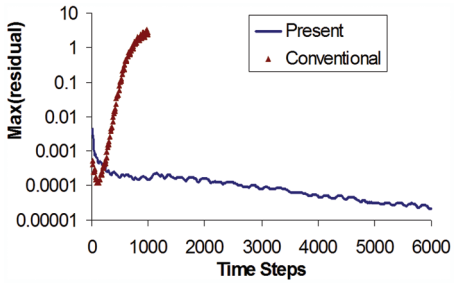

Fig. 9 Convergence histories of the present harmonic solver and a conventional time-linearized one (turbine cascade subject to incoming unsteady wake disturbances).

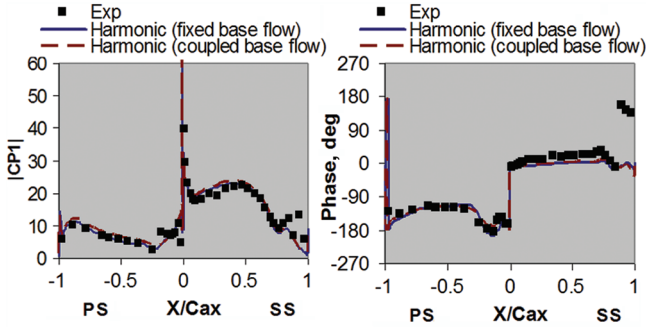

Fig. 10 Unsteady pressure amplitude and phase angle (turbine cascade oscillating around midchord, torsion amplitude 1 deg, reduced frequency 0.7, mean inflow angle 40 deg).

from the experimental data [32] showing that the longest separation bubble covering more than 50% chord occurs at the most negative incidence condition (20 deg inflow angle). The prescribed blade oscillation movement is in a torsion mode around the midchord with an amplitude of 1 deg. The reduced frequency based on the exit flow velocity is 0.7. The interblade phase angle is 180 deg. The computed unsteady harmonic pressures are compared with the corresponding experimental data as shown in Figs. 10 and 11. Both the amplitudes and phase angles agree very well with the experimental data. Noticeable discrepancies appear in the phase angle on the suction surface near the trailing edge. The local sudden jump in the phase angle as shown in the experimental data is attributed to unsteady movement of the reattachment point of the short separation bubble on the suction surface. This can be reasonably predicted by using a quasi-steady transition model for short separation bubbles [33] but is

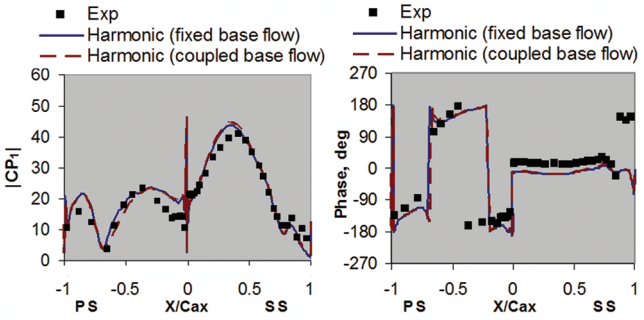

Fig. 11 Unsteady pressure amplitude and phase angle (turbine cascade oscillating around midchord, torsion amplitude 1 deg, reduced frequency 0.7, mean inflow angle 20 deg).

not attempted here. The flow is tripped at the leading edge and assumed to be turbulent on the blade surfaces. The significant unsteady loading from the leading edge to 60% chord, attributed to the long separation bubble on the pressure surface at the inflow angle of 20 deg, is well captured (Fig. 11).

Also shown in Figs. 10 and 11 are the results with the base flow being coupled together with the harmonic solutions, this is, solving Eqs. (8) and (9) simultaneously. For the present cases, even with a large-scale flow separation, the results of the fully coupled harmonic solutions are nearly the same as those with the base flow being fixed at the steady state. Hence, the unsteady flow due to the blade vibration is largely linear. Starting from a steady solution, the fully coupled solution (equivalent to three steady solutions) is 50% more time consuming than that with a fixed steady field as the base flow. Clearly, the harmonic solution with a fixed base-flow state has the advantage when the mean flow is not significantly changed by nonlinearity. The relatively insignificant nonlinear effects on the unsteady-flow response for this highly separated flow case as observed here are consistent with the previous study using a nonlinear time-marching solver [33].

C. High-Speed Oscillating Turbine Cascade with Flow Separation

This is the eleventh test case (denoted as STCF11) as part of the standard test configurations documented by Fransson et al. [34]. The annular cascade of turbine blading is tested at a transonic condition with an inflow angle of 34 deg and an exit Mach number of 0.96. The blades are mechanically driven to oscillate in a flapping mode at a prescribed frequency and interblade phase angle.

The calculated steady-flow surface pressure distributions in terms of the isentropic Mach number are in a good agreement with the experimental data, as shown in Fig. 12. The exit flow angle is about 60 deg and, hence, the overall flow turning is over 90 deg at this condition. The very high incidence results in a long separation bubble, indicated by the entropy contours (Fig. 13a) and confirmed by the local streamlines, superimposed on the static pressure contours (Fig. 13b). This leading-edge separation bubble presents a challenge to the convergence of conventional linearized solvers. Campobasso and Giles [21] show that, for this test case, the pseudomarching of the time-linearized solver quickly leads to a

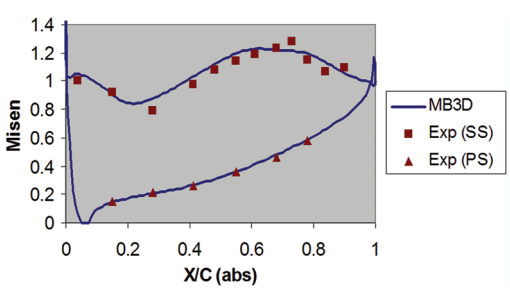

Fig. 12 Steady surface pressure (isentropic Mach number) distributions for transonic turbine cascade (STCF11, inflow angle 34 deg, exit Mach number 0.99).

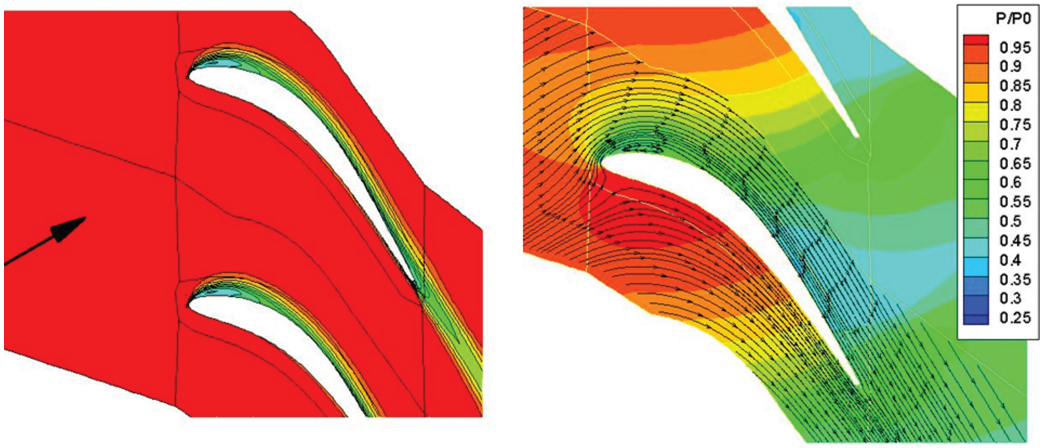

a) Total pressure loss b) Static pressure (lower passage with streamlines)

Fig. 13 Steady-flow results for transonic turbine cascade (STCF11, inflow angle 34 deg, exit Mach number 0.99).

solution divergence, and a convergence can only be achieved by a GMRES stabilization technique implemented in their time-linearized solver.

With the base flow subject to the large-scale leading-edge separation bubble, the present harmonic solver does not experience a convergence problem. The convergence history of the harmonic solution is shown in Fig. 14. The maximum residual is shown to drop by 3 orders of magnitude with about 2000 time-marching steps.

The unsteady pressure distributions (harmonic amplitude and phase angles) on the blade surface are shown in Fig. 15. The computed results compare well with the corresponding experimental data and are comparable to those of other nonlinear flow solvers (Fransson et al. [34]) and stabilized time-linearized methods (Campobasso and Giles [21]) for this transonic flow case.

It is of interest to examine the effect of fixing the steady flow as the base flow for unsteady perturbations at this transonic condition with separation. A harmonic solution is also carried out with the base flow coupled with the unsteady harmonic part, the three phase solutions being simultaneously solved at $\omega t = 0, -90$, and 90 deg. The results are also presented in Fig. 15. The comparison shows little difference, suggesting that coupling harmonic unsteadiness with the base flow with the extra 50% computing effort does not improve the accuracy, even for this transonic flow with large-scale separation. Thus, the unsteady response is largely linear. This again illustrates the advantage of the present harmonic approach in terms of computational efficiency, particularly for a blade aeromechanical analysis in which unsteady load response at a single frequency of a given structural vibration mode is needed.

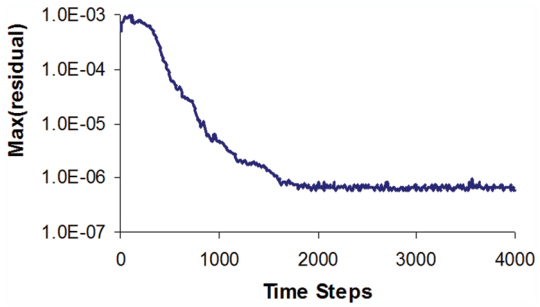

Fig. 14 Convergence history of the present harmonic solver for transonic oscillation cascade with large-scale separation (STCF11, inflow angle 34 deg, exit Mach number 0.99).

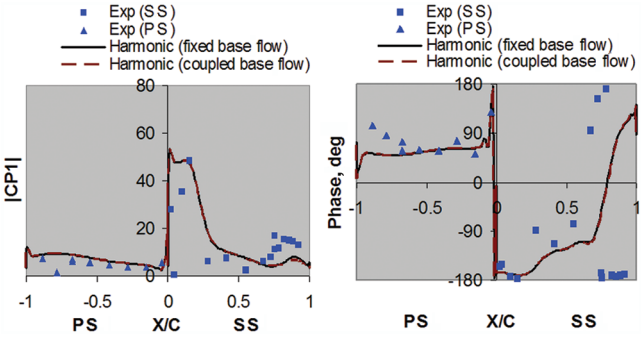

Fig. 15 Unsteady pressure amplitude and phase angle for transonic oscillating turbine cascade (STCF11, inflow angle 34 deg, exit Mach number 0.99, IBPA = 180 deg).

IV. Conclusions

Time-linearized frequency-domain methods have been extensively developed for many applications for which unsteady disturbances at a given frequency need to predicted, for example, for turbomachinery aeromechanics and aeroacoustics. For highly loaded flow conditions, local flow separation may be unavoidable. The base flow, typically solved using a nonlinear steady-flow solver, may then exhibit limit-cycle types of instabilities, and the linearized harmonic solution will experience convergence difficulties. There are remedies (e.g., GMRES) recently developed, but they are often complex with extra penalties in computer memory. In the present work, a simple real-number formulation is adopted for modeling harmonic disturbances, aimed at harnessing nonlinearity efficiently for the stabilization of time harmonic solutions. One unsteady complex-number harmonic solution is made equivalent to two real-number steady-flow solutions with simple source terms. The method is verified against a semi-analytical theory for an unsteady wake induced flow in a flat plate cascade. Further validations are conducted for low- and high-speed turbine cascades. The results are in good agreement with the corresponding experimental data. The computational results show that the new harmonic solver is very robust with much improved convergence over the conventional time-linearized method. It is clearly demonstrated that converged solutions can be very effectively obtained using the present method for flows with large-scale separation.

Appendix: Comparative Harmonic Formulations for a Nonlinear Model Equation

Take the 1-D convection equation

$$\frac{\partial u}{\partial t} + \frac{1}{2}\frac{\partial u^2}{\partial x} = 0 \tag{A1}$$

Assume that an unsteadiness is a small perturbation to a steady state:

$$u = u_o(x) + u_1(x,t) \tag{A2}$$

Substitute u in Eq. (A3) into the original equation [Eq. (A1)] and we have

$$\frac{\partial u_1}{\partial t} + \frac{1}{2}\frac{\partial}{\partial x}(u_o^2 + 2u_0u_1 + u_1^2) = 0 \tag{A3}$$

The nonlinear term for the unsteady fluctuation u_1^2 is a second-order term. The conventional time linearization is realized by neglecting this nonlinear second-order term. Then we have

$$\frac{1}{2}\frac{\partial u_o^2}{\partial x} + \frac{\partial u_1}{\partial t} + \frac{\partial}{\partial x}(u_0u_1) = 0 \tag{A4}$$

Equation (A4) will be satisfied if

$$\frac{\partial u_o^2}{\partial x} = 0 \tag{A5a}$$

and:

$$\frac{\partial u_1}{\partial t} + \frac{\partial}{\partial x}(u_0u_1) = 0 \tag{A5b}$$

Equation (A5a) is the steady-state equation and Eq. (A5b) is a linear equation for the unsteady perturbation once the steady solution is obtained. Now introduce a real-number temporal Fourier harmonic expression with one harmonic:

$$u_1(x,t) = A_u \cos\omega t + B_u \sin\omega t \tag{A6}$$

Substitute Eq. (A6) into Eq. (A5b). Balancing all the terms with $\cos\omega t$ and $\sin\omega t$, respectively, we then have two time-independent linear equations for the two harmonic coefficients:

$$B_u\omega + \frac{\partial}{\partial x}(u_0A_u) = 0 \tag{A7a}$$

$$-A_u\omega + \frac{\partial}{\partial x}(u_0B_u) = 0 \tag{A7b}$$

The present nonlinear harmonic formulation would start with the nonlinear time-domain equation [Eq. (A3)]. Now with the harmonic expression of the perturbation [Eq. (A6)], the nonlinear equation becomes

$$\begin{aligned} &-A_u\omega\sin\omega t + B_u\omega\cos\omega t \\ &+\frac{1}{2}\frac{\partial}{\partial x}\Big[u_o^2 + 2u_0(A_u\cos\omega t + B_u\sin\omega t) \\ &+(A_u\cos\omega t + B_u\sin\omega t)^2\Big] = 0 \end{aligned} \tag{A8}$$

Taking Eq. (A8) at the two distinctive temporal phase angles ($\omega t = 0$ and 90 deg), respectively, we then have

$$B_u\omega + \frac{1}{2}\frac{\partial}{\partial x}\Big[u_o^2 + 2u_0A_u + (A_u)^2\Big] = 0 \tag{A9a}$$

$$-A_u\omega + \frac{1}{2}\frac{\partial}{\partial x}\Big[u_o^2 + 2u_0B_u + (B_u)^2\Big] = 0 \tag{A9b}$$

Although these are similar to the conventional time-linearized counterparts [Eq. (A7)], they are clearly nonlinear even for a given steady state u_0.

References

[1] Graf, M. B., Greitzer, E. M., Marble, F. E., and Sharma, O. P., "Effects of Stator Pressure Field on Upstream Rotor Performance," American Society of Mechanical Engineers Paper 99-GT-99, 1999.

[2] Lane, F., "System Mode Shapes in Flutter of Compressor Blade Rows," *Journal of the Aeronautical Sciences*, Vol. 23, No. 1, 1956, pp. 54–66.

[3] Whitehead, D. S., "Force and Moment Coefficients for Vibrating Aerofoils in Cascade," Aeronautical Research Council, R&M Rept. 3254, 1962.

[4] Atassi, H., and Akai, T. J., "Aerodynamics Force and Moment in Oscillating Aerofoils in Cascade," American Society of Mechanical Engineers Paper 78-GT-181, 1978.

[5] Adamczyk, J. J., and Goldstein, M. E., "Unsteady Flow in a Supersonic Cascade with Leading-Edge Locus," *AIAA Journal*, Vol. 16, No. 12, 1978, pp. 1248–1254.

[6] Ni, R. H., and Sisto, F., "Numerical Computation of Nonstationary Aerodynamics of Flat Plate Cascade in Compressible Flow," American Society of Mechanical Engineers Paper 75-GT-5, 1975.

[7] Verdon, J. M., "Analysis of Unsteady Supersonic Cascades," American Society of Mechanical Engineers Paper 77-GT-44, 1977.

[8] Namba, M., "Lifting Surface Theory for Rotating Subsonic or Transonic Blade Row," Aeronautical Research Council, R&M Rept. 3740, 1972.

[9] Whitehead, D. S., "The Calculations of Steady and Unsteady Transonic Flow in Cascades," Cambridge University Engineering Department Rept. CUED/A-Turbo/TR118, 1982.

[10] Verdon, J. M., and Caspar, J. R., "Development of a Linear Unsteady Aerodynamics for Finite-Deflection Cascades," *AIAA Journal*, Vol. 20, No. 9, 1982, pp. 1259–1267.

[11] Hall, K. C., and Crawley, E. F., "Calculation of Unsteady Flows in Turbomachinery Using the Linearized Euler Equations," *AIAA Journal*, Vol. 27, No. 6, 1989, pp. 777–787.

[12] Hall, K. C., and Lorence, C. B., "Calculation of Three Dimensional Unsteady Flows in Turbomachinery Using the Linearized Harmonic Euler Equations," *Journal of Turbomachinery*, Vol. 115, No. 4, 1993, pp. 800–809.

[13] Clark, W. S., and Hall, K. C., "A Time-Linearised Navier–Stokes Analysis of Stall Flutter," *Journal of Turbomachinery*, Vol. 122, No. 3, 2000, pp. 467–476. doi:10.1115/1.1303073

[14] Sbardella, L., and Imregun, M., "Linearised Unsteady Viscous Turbomachinery Flows on Hybrid Grids," *Journal of Turbomachinery*, Vol. 123, No. 3, 2001, pp. 568–582. doi:10.1115/1.1371777

[15] He, L., "An Euler Solution for Unsteady Flows Around Oscillating Blades," *Journal of Turbomachinery*, Vol. 112, No. 4, 1990, pp. 714–722.

[16] Dewhurst, S., and He, L., "Unsteady Flow Calculations Through Turbomachinery Stages Using Single-Passage Domain with Shape-Correction Method," *Proceedings of the 9th International Symposium on Unsteady Aerodynamics and Aeroelasticity in Turbomachines*, edited by P. Ferrand and S. Aubert, Press of University of Grenoble, Grenoble, France, Sept. 2000, pp. 338–350.

[17] Gerolymos, G. A., Michon, G. J., and Neubauer, J., "Analysis and Application of Chorochronic Periodicity in Turbomachinery Rotor/Stator Interaction Computations," *Journal of Propulsion and Power*, Vol. 18, No. 6, 2002, pp. 1139–1152.

[18] Ning, W., and He, L., "Computation of Unsteady Flows Around Oscillating Blades Using Linear and Non-Linear Harmonic Euler Methods," *Journal of Turbomachinery*, Vol. 120, No. 3, July 1998, pp. 508–514.

[19] Hall, K. C., Thomas, J., and Clark, W. S., "Computation of Unsteady Nonlinear Flows in Cascades Using a Harmonic Balance Technique," *AIAA Journal*, Vol. 40, No. 5, 2002, pp. 878–886.

[20] McMullen, M. S., Jameson, A., and Alonso, J., "Application of a Non-Linear Frequency-Domain Solver to the Euler and Navier–Stokes Equations," AIAA Paper 2002-0120, Jan. 2002.

[21] Campobasso, M. S., and Giles, M. B., "Effects of Flow Instabilities on The Linear Analysis of Turbomachinery Aeroelasticity," *Journal of Propulsion and Power*, Vol. 19, March–April 2003, pp. 250–259.

[22] Sparlart, P. R., and Allmaras, S. R., "A One-Equation Turbulence Model for Aerodynamic Flows," AIAA Paper 92-0439, Jan. 1992.

[23] Hoffmann, K., Chiang, S., Siddiqui, S., and Papadakis, M., *Fundamental Equations of Fluid Mechanics*, Engineering Education Systems, Wichita, KS, 1996.

[24] Jameson, A., "Time-Dependent Calculations Using Multi-Grid, with Applications to Unsteady Flows Past Airfoil and Wings," AIAA Paper 91-1596, Jan. 1991.

[25] Adamczyk, J. J., "Model Equations for Simulating Flows in Multistage-Turbomachinery," American Society of Mechanical Engineers Paper 85-GT-226, June 1985.

[26] Ning, W., and He, L., "Some Modelling Issues on Trailing Edge Vortex Shedding," *AIAA Journal*, Vol. 39, No. 5, May 2001, pp. 787–793.

[27] Jameson, A., Schmidt, W., and Turkel, E., "Numerical Solutions of the Euler Equation by Finite Volume Method Using Runge–Kutta Time-Stepping Scheme," AIAA Paper 81-1259, Jan. 1981.

[28] Giles, M. B., "Non-Reflecting Boundary Conditions for the Euler Equations," *AIAA Journal*, Vol. 28, No. 12, 1990, pp. 2050–2058.

[29] Whitehead, D. S., "Classical Two-Dimensional Methods," *AGARD Manual on Aeroelasticity in Axial Flow Turbomachines, Unsteady Turbomachinery Aerodynamics*, Vol. 1, Chap. 3, AGARD-AG-298, edited by M. F. Platzer and F. O. Carta, Neuilly Sur Seine, France, March 1987.

[30] Chen, T., Vasanthakumar, P., and He, L., "Analysis of Unsteady Blade Row Interaction Using Nonlinear Harmonic Approach," *Journal of Propulsion and Power*, Vol. 17, No. 3, May 2001, pp. 651–658.

[31] Hodson, H. P., and Dawes, W. N., "On Interpretation of Measured Profile Losses Iin Unsteady Wake-Turbine Blade Interaction Studies," *Journal of Turbomachinery*, Vol. 120, No. 2, 1998, pp. 276–282.

[32] He, L., "Unsteady Flow in Oscillating Turbine Cascade, Part 1. Linear Cascade Experiment," *Journal of Turbomachinery*, Vol. 120, No. 2, 1998, pp. 262–275.

[33] He, L., "Unsteady Flow in Oscillating Turbine Cascade, Part 2. Computational Study," *Journal of Turbomachinery*, Vol. 120, No. 2, 1998, pp. 262–275.

[34] Fransson, T. H., Joeker, M., Boelcs, A., and Ott, P., "Viscous and Inviscid Linear/Nonlinear Calculations Versus Quasi Three-Dimensional Experimental Cascade Data for a New Aeroelastic Turbine Standard Configuration", *Journal of Turbomachinery*, Vol. 121, No. 4, Oct. 1999, pp. 717–725.

R. Rangel
Associate Editor